Realization of all-crystalline GaN/Er:GaN/GaN core-cladding optical fiber structures

View Online   Export Citation   CrossMark

T. B. Smith, Y. Q. Yan, W. P. Zhao, J. Li, J. Y. Lin, and H. X. Jiang[a]

AFFILIATIONS

Department of Electrical and Computer Engineering, Texas Tech University, Lubbock, Texas 79409, USA

[a]Author to whom correspondence should be addressed: hx.jiang@ttu.edu

ABSTRACT

Erbium-doped gallium nitride (Er:GaN) is a promising gain material for solid-state high-energy lasers operating in the 1.5 μm wavelength window due to the superior optical properties and extremely high thermal conductivity of a GaN host crystal that permit high-power and high-temperature applications. We report the realization of all-crystalline GaN/Er:GaN/GaN embedded waveguide fiber structures using the hydride vapor phase epitaxy growth and re-growth technique, along with chemical–mechanical polishing processes. The Er:GaN core layer possesses an Er doping concentration of 1.7×10^{20} atoms/cm^3, confirmed by secondary ion mass spectrometry measurements. X-ray diffraction measurements confirm, respectively, c-, a-, and m-plane orientations for top/bottom, side, and front/back cross-sectional cladding layers of the fiber structure with good single-crystalline quality. The 1.5 μm Er^{3+} emission was detected from each surface of the fiber structures via 980 nm resonant excitation. The effect of 1.54 μm light guiding by the fiber structure has been demonstrated. This work laid the foundation toward achieving all-crystalline core-cladding fibers based on GaN wide bandgap semiconductor with potential applications in the harsh environments of high powers, power densities, and temperatures.

Tremendous progress in solid-state high-energy lasers (HELs) have been made due to an immense range of applications that include communications, defense, medicine, spectroscopy, and industrial/commercial processing.[1] HELs operating at the 1.5 μm wavelength window are particularly desired as this wavelength range provides high atmospheric transmission, corresponds to the absorption minimum in silica optical fibers, and is considered eye-safe as the light is strongly absorbed in the surface of the eye and, therefore, will not reach the retina.[2] The emission wavelength and performance of a HEL system are predominantly determined by the optical gain medium. Rare earth doped GaN, including erbium-doped GaN (Er:GaN) emitting at 1.5 μm, possessing excellent optical, mechanical, and thermal properties have shown to be an excellent gain medium.[3–11] Erbium-doped YAG (Er:YAG) and erbium-doped optical fiber amplifiers (EDFAs) are also used as gain media operating at 1.5 μm but are limited by properties of the host materials, such as low thermal conductivity ($\kappa = 17$ W/m K) and large thermal expansion coefficient ($\alpha = 8 \times 10^{-6\,\circ}$C^{-1}).[12,13] EDFAs are composed of amorphous glasses with limited diameters that rely on heat dissipation over long fiber lengths and suffer from thermal quenching at shorter lengths that require higher doping concentrations. GaN, a wide bandgap semiconductor, has a relatively low thermal expansion coefficient ($\alpha = 3.53 \times 10^{-6\,\circ}$C^{-1}) and extremely high

thermal conductivity ($\kappa = 253$ W/m K).[14] Furthermore, the wide bandgap of GaN results in low thermal quenching of the 1.5 μm Er emission.[9] The superior host properties of GaN potentially allow for higher operating powers and temperatures than the traditional gain media, making Er:GaN a promising candidate for use in HEL systems.

Among various waveguide structures, core-cladding planar waveguide (PWG) structures are the preferred geometry for gain media in HELs, owing to their large surface areas that allow for efficient heat removal during high-power/high-temperature applications and ease of optical pumping.[15–21] We have previously reported the growth and fabrication process and subsequent optical studies of GaN/Er:GaN/GaN core-cladding PWGs by the hydride vapor phase epitaxy (HVPE) growth method.[22,23]

Recently, semiconductor core optical fiber (SCFs) structures have been investigated due to their ability to provide optical confinement in all dimensions with improved performance compared to PWGs.[24–26] The majority of these structures rely on fabrication using molten core methods (MCMs) where the core layer is pulled slowly from a fluid melt and crystallizes at a predetermined diameter. These methods and post-processing treatments allow for single-crystalline quality of the core layer; however, cladding materials for SCFs are generally limited to glasses and polycrystalline materials as the MCMs cannot be
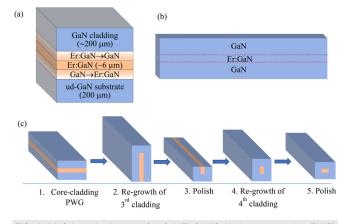
FIG. 1. (a) Schematic diagram of a GaN/Er:GaN/GaN planar waveguide (PWG) structure, (b) schematic diagram of a GaN/Er:GaN/GaN core-cladding fiber structure, and (c) schematic diagram showing the fabrication process of GaN/Er:GaN/GaN core-cladding fiber structures from PWGs.

repeated without remelting the core again.[24] Therefore, it is exceedingly difficult to fabricate all-crystalline optical fibers in which both the core and cladding are single crystals.

In this work, we report the realization of an all-crystalline GaN/Er:GaN/GaN embedded waveguide fiber structure by HVPE. The HVPE growth technique was employed due to the ability to synthesize high-quality GaN layers at growth rates of 100's μm/h. The HVPE system used in this work and the fabrication processes for all-crystalline GaN/Er:GaN/GaN PWGs have been reported previously.[22] The fiber structures were fabricated from GaN/Er:GaN/GaN PWGs after processing by chemical–mechanical polishing (CMP) of the sidewalls. Schematic diagrams of the PWG structure and the fiber structure are shown in Figs. 1(a) and 1(b), respectively. The fabrication of the all-crystalline core-cladding fiber structure follows the basic processing flow shown in Fig. 1(c): (1) the process to fabricate the fiber structure started from the PWG structure. (2) The PWG structure was placed in the HVPE reactor, with one sidewall facing upward, for the growth of the third cladding layer of 400 μm in thickness on the a-plane surface. (3) After growth of the third cladding layer, the remaining exposed sidewall was polished, leaving the desired width of the fiber core layer remaining. (4) The polished structure was placed back in the HVPE reactor for re-growth of the fourth cladding layer, 400 μm in thickness, on the final a-plane surface. (5) To finish the fiber structure, each of the two cross-sectional m-plane surfaces and four cladding surfaces were polished to appropriate thicknesses and mirror-finishing. The completed fiber structures are composed of a rectangular Er:GaN core with a cross-sectional area of 6 × 200 μm^2, surrounded by ~200 μm of undoped GaN cladding on each side.

An optical image of a finished fiber structure is shown in Fig. 2(a). It is worth noting due to the wurtzite structure of GaN, if an all-crystalline fiber is obtained, the short side of the rectangular fiber structure is parallel to the a-axis of GaN, as illustrated in Fig. 2(b), resulting in m-plane GaN orientation for the cross-sectional faces of the fiber structure and a-plane GaN orientation for each of the side cladding layers. The crystallographic orientation of each surface of the fiber structure is shown in Fig. 2(c). The A_1 and A_2 a-plane GaN cladding layers were grown in the (11$\bar{2}$0) and ($\bar{1}\bar{1}$20) directions,
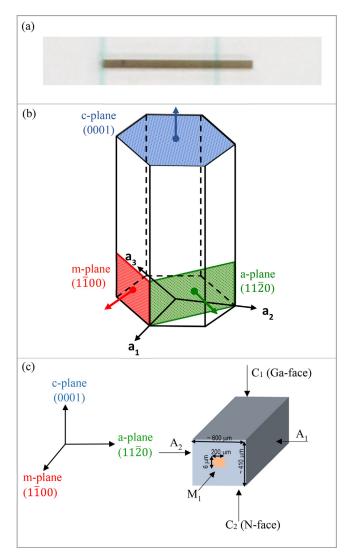

FIG. 2. (a) Optical image of a finished fiber structure (top view), (b) schematic illustration of different crystal planes of wurtzite GaN, and (c) schematic illustration of the crystallographic orientations and surfaces of the fabricated fiber structure composed of a rectangular Er:GaN core with a cross-sectional area of 6 × 200 μm^2, surrounded by ~200 μm of undoped GaN cladding on each side (dimensions are not to scale).

respectively. The m-plane GaN cross-sectional faces of the fiber structure were polished flat to the (1$\bar{1}$00) and ($\bar{1}$100) directions.

X-ray diffraction (XRD) measurements were performed on each face of the fiber structure to confirm the crystallographic orientation and verify that an all-crystalline fiber has been achieved. Figure 3(a) shows the XRD θ–2θ scan of the first cladding layer c-plane GaN (0002), exhibiting a peak at 34.553°, in comparison with the peak position of strain-free GaN at 34.569°, which indicates that strain is comparable to the Er:GaN layer underneath. The full-width-at-half maxima (FWHM) of θ–2θ [Fig. 3(a)] and rocking curve (RC) [Fig. 3(b)] scans of 97.2 and 324 arc sec, respectively, indicate good

FIG. 3. X-ray diffraction spectra of the (a) θ–2θ scan, (b) ω-scan or rocking curve (RC) of the (0002) reflection peak, (c) and polycrystal scan (5° offset with respect to the c-axis of GaN) of the top GaN cladding layer (C_1).

FIG. 4. X-ray diffraction spectra of the (a) θ–2θ scan, (b) ω-scan or rocking curve (RC) of the (11$\bar{2}$0) reflection peak, (c) and polycrystal scan (5° offset with respect to the a-axis of GaN) for a side GaN cladding layer (A_1).

crystalline quality. The broad background peak of the RC is likely due to contributions from the core and side cladding layers. More importantly, the θ–2θ polycrystal scan (5° off-axis) shown in Fig. 3(c) reveals no other peaks implying no polycrystalline domains were detected.

The XRD θ–2θ scan of the A_1 cladding layer GaN (11$\bar{2}$0) peak shown in Fig. 4(a) exhibits a position at 57.735° that is near the expected position of 57.774°, confirming the growth of single-crystalline GaN in a-plane orientation for the A_1 and A_2 cladding layers. The XRD RC of the A_1 cladding layer shown in Fig. 4(b) exhibits multiple peaks with a large FWHM of 1310 arc sec, which is a result of the difficulty in polishing the fiber sides parallel to the a-plane before regrowth of the side cladding layers. The θ–2θ polycrystal scan (5° off-axis) shown in Fig. 4(c) again confirms no polycrystalline domains were detected. The θ–2θ scan of the fiber cross section GaN (1$\bar{1}$00) peak at 32.364° shown in Fig. 5(a) is also near the expected position of 32.390°, confirming m-plane orientated GaN for the cross-sectional faces. The RC scan of the fiber cross section shown in Fig. 5(b) exhibits FWHM of 335 arc sec, indicating a higher crystalline quality of the m-plane GaN cladding layers compared to that of the a-plane GaN cladding layer surface, due to the higher quality of the c-plane GaN cladding layers. Lower RC intensities observed for the m-plane GaN cladding layers are the result from a smaller cross-sectional area measured. Again, no polycrystalline growth is detected in the scans of fiber cross section, as confirmed by the polycrystal scan (5° off-axis) shown in Fig. 5(c). The XRD results
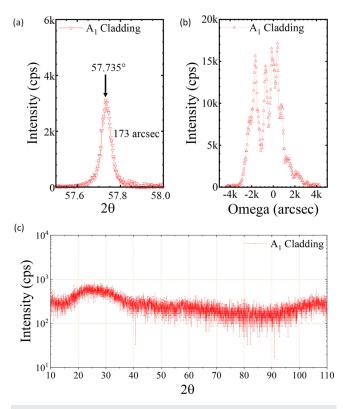
shown in Figs. 3–5 conclusively confirm the realization of an all-crystalline Er:GaN/GaN core-cladding fiber structure.

To confirm the Er incorporation in the core, room-temperature photoluminescence (PL) studies were performed to verify the 1.5 μm emission that originates from optical transitions between the first excited state ($^4I_{13/2}$) to the ground state ($^4I_{15/2}$) of the Er^{3+} ion under 980 nm resonant excitation, which excites carriers from the $^4I_{15/2}$ ground state to the $^4I_{11/2}$ excited state manifolds of Er^{3+} ions. The 980 nm excitation photons and emitted 1.5 μm photons are transported by a 400 μm bifurcated optical fiber located directly beneath the sample. Figure 6 compares the PL emission spectra measured from the cross-sectional face and each undoped GaN cladding layer of the finished fiber structure. The PL spectra from each surface show similar emission shape while the emission from the C_1 cladding layer exhibits the highest intensity, primarily due to the large cross-sectional area of the Er doped core layer, emissions from the A_1 and A_2 cladding layers are reduced by more than a factor of 5, and emission from the cross section is reduced by more than a factor of 10. The difference in PL emission intensities observed for the C_1 and C_2 cladding layers, by a factor of 2, is most likely related to the Ga-polar and N-polar orientations of C_1 and C_2 cladding layers. The reductions in emission intensity for the A_1 and A_2 cladding layers and the cross-sectional surface, compared to the C cladding layers, are a factor of the small cross-sectional area (6 × 200 μm^2) of Er:GaN core. Secondary ion mass spectrometry (SIMS) measurement was conducted to evaluate the Er
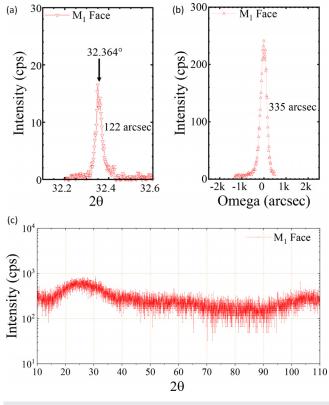
FIG. 5. X-ray diffraction spectra of the (a) θ–2θ scan, (b) ω-scan or rocking curve (RC) of the ($1\bar{1}00$) reflection peak, (c) and polycrystal scan (5° off with respect to the m-axis of GaN) for a GaN cladding on the cross-sectional face (M_1).
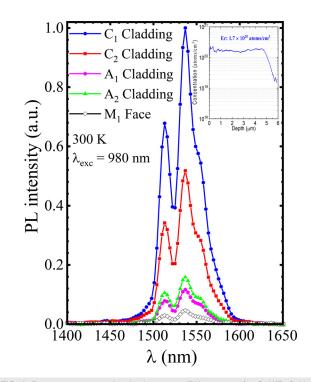

FIG. 6. Room temperature photoluminescence (PL) spectra of a GaN/Er:GaN all-crystalline fiber measured around 1.5 μm, under resonant excitation ($\lambda_{exc} = 980$ nm), from each surface of the finished fiber structure. The inset of Fig. 6 shows the profile of Er concentration in the Er:GaN core layer measured by SIMS, revealing an Er concentration of 1.7×10^{20} atoms/cm^3 in the core.

doping concentration throughout the Er:GaN core layer. The SIMS results shown in the inset of Fig. 6 indicate an average Er concentration of 1.7×10^{20} atoms/cm^3 in the core. The Er concentration decreases gradually in the transition layer, as expected. As illustrated in Fig. 1(a), the growth of the PWG begins as undoped GaN and the Er doping is gradually increased to the desired concentration before uniform growth of the Er:GaN core layer was employed. The single-crystalline nature of the Er:GaN core has been demonstrated previously.[22] With an Er doping concentration of 1.7×10^{20} atoms/cm^3 in the core, the estimated confinement factor for a 6 μm thick core is about 95%.[23]

Waveguiding and transmission characteristics of the fiber structure at 1.54 μm were also investigated. The 1.54 μm laser beam was focused onto the M_1 face of the fiber structure and the transmitted laser beam profile was then recorded using an infrared (IR) CCD camera placed approximately 1 cm behind the exit facet of the fiber. In order to demonstrate the waveguiding effect, measurements were performed in two configurations: (1) the fiber axis is parallel with the propagation direction of the incoming 1.54 μm laser beam (angle of incidence $\theta_i = 0°$) and (2) the fiber structure is rotated and the incoming 1.54 μm enters M_1 face at $\theta_i > 0°$. If waveguiding is achieved, the detected output from the exit facet of the fiber structure should shift horizontally with increasing θ_i. Figure 7(a) shows the gray-level histogram of the measurement data obtained at $\theta_i = 0°$ (red circles) and

$\theta_i = 5°$ (blue squares). The detected laser profile shifted approximately 1.9 mm in the horizontal direction, agreeing with the amount of angle shift for the fiber.

The polarization dependence of the transmitted 1.54 μm light was studied by inserting a polarizer between the exit facet of the waveguide and the IR CCD camera. Figure 7(b) shows the gray-level histogram comparing the relative transmitted intensities of TM and TE mode polarizations. The TM mode transmission is approximately 2.5 times greater than the transmission of TE mode, accounting for 63% of the transmitted light. The results further demonstrated the waveguiding effect. However, further investigations are needed to understand the loss mechanisms in the fiber structures of different crystallographic orientations.

In summary, the fabrication of an all-crystalline GaN/Er:GaN/GaN embedded waveguide fiber has been realized using the HVPE regrowth method. XRD measurements confirm single-crystalline quality of both the core and cladding layers as well as the expected crystallographic orientation of the a-plane GaN side cladding layers and the m-plane GaN cross-sectional surface. The HVPE GaN cladding regrowth along the a-plane and m-plane also demonstrates high crystalline quality. The incorporation of Er in the core is confirmed by the detection of 1.5 μm Er^{3+} emission from each surface of the fiber structure via a resonant excitation using a 980 nm laser diode as well as by the SIMS measurements, revealing an Er doping concentration of 1.7×10^{20} atoms/cm^3 in the Er:GaN core layer. The transmission of a 1.54 μm laser beam through the fiber structure demonstrates an
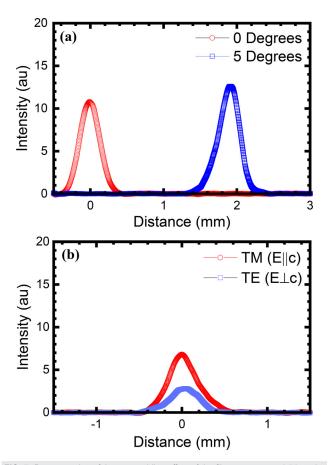
FIG. 7. Demonstration of the waveguiding effect of the fiber structure at 1.54 μm by focusing a 1.54 μm laser beam onto the M_1 face of the fiber structure with an IR CCD camera placed behind the exit facet of the fiber to detect the output profiles. (a) The gray-level histogram of the transmitted laser beam profiles obtained when the fiber structure was rotated with its axis changing from parallel (red circles) to a 5° angle (blue squares) in reference to the incoming laser beam. (b) The polarization dependence of the transmitted 1.54 μm light.

effective waveguiding and a polarization dependence, with TM-mode transmission nearly 2.5 times greater than TE-mode. The realization of these fiber structures represents a significant step toward achieving all-crystalline core-cladding fibers based on Er-doped GaN wide bandgap semiconductors that can be utilized in applications of harsh environments of high powers, high power densities, and high temperatures.

AUTHOR DECLARATIONS
Conflict of Interest

The authors have no conflicts to disclose.

Author Contributions

Trey Brendan Smith: Investigation (equal); Methodology (equal); Validation (equal); Writing – original draft (equal). **Yaqiong Yan:** Investigation (equal); Methodology (equal). **Weiping Zhao:** Investigation (equal). **Jing Li:** Investigation (equal); Methodology (equal); Supervision (equal). **Jingyu Lin:** Conceptualization (equal); Data curation (equal); Formal analysis (equal); Funding acquisition (equal); Investigation (equal); Methodology (equal); Project administration (equal); Resources (equal); Supervision (equal); Validation (equal); Visualization (equal); Writing – original draft (equal); Writing – review & editing (equal). **Hongxing Jiang:** Conceptualization (equal); Data curation (equal); Formal analysis (equal); Funding acquisition (equal); Investigation (equal); Methodology (equal); Project administration (equal); Resources (equal); Supervision (equal); Validation (equal); Visualization (equal); Writing – original draft (equal); Writing – review & editing (equal).

DATA AVAILABILITY

The data that support the findings of this study are available within the article.

REFERENCES

[1] Y. Kalisky and O. Kalisky, Opt. Eng. **49**, 091003 (2010).
[2] J. A. Zuclich, D. J. Lund, and B. E. Stuck, Health Phys. **92**, 15 (2007).
[3] R. G. Wilson, R. N. Schwartz, C. R. Abernathy, S. J. Pearton, N. Newman, M. Rubin, T. Fu, and J. M. Zavada, Appl. Phys. Lett. **65**, 992 (1994).
[4] A. J. Steckl, J. C. Heikenfeld, D. S. Lee, M. J. Garter, C. C. Baker, Y. Wang, and R. Jones, IEEE J. Sel. Top. Quantum Electron. **8**, 749 (2002).
[5] A. J. Steckl and J. M. Zavada, MRS Bull. **24**, 33 (1999).
[6] V. Dierolf, *Rare-Earth Doped III-Nitrides for Optoelectronic and Spintronic Applications*, edited by K. O'Donnell and V. Dierolf (Canopus Academic Publishing Ltd.—Springer SBM, 2010), Chap. 8.
[7] A. Braud, *Rare-Earth Doped III-Nitrides for Optoelectronic and Spintronic Applications*, edited by K. O'Donnell and V. Dierolf (Canopus Academic Publishing Ltd.—Springer SBM, 2010), Chap. 9.
[8] Y. Fujiwara and A. Koizumi, Rev. Laser Eng. **42**, 211 (2014).
[9] Z. Y. Sun, J. Li, W. P. Zhao, J. Y. Lin, and H. X. Jiang, Appl. Phys. Lett. **109**, 052101 (2016).
[10] C. Ugolini, N. Nepal, J. Y. Lin, H. X. Jiang, and J. M. Zavada, Appl. Phys. Lett. **89**, 151903 (2006).
[11] D. W. Jeon, Z. Y. Sun, J. Li, J. Y. Lin, and H. X. Jiang, Opt. Mat. Express **5**, 596 (2015).
[12] R. Wynne, J. L. Daneu, and T. Y. Fan, Appl. Opt. **38**, 3282 (1999).
[13] W. Xie, S.-C. Tam, H. Yang, J. Gu, G. Zhao, Y. L. Lam, and W. Tan, Opt. Laser Technol. **31**, 521 (1999).
[14] H. Shibata, Y. Waseda, H. Ohta, K. Kiyomi, K. Shimoyama, K. Fujito, H. Nagaoka, Y. Kagamitani, R. Simura, and T. Fukuda, Mater. Trans. **48**, 2782 (2007).
[15] H. Chen, H. Fu, X. Huang, X. Zhang, T. H. Yang, J. A. Montes, I. Baranowski, and Y. Zhao, Opt. Express **25**, 31758 (2017).
[16] T. Sekiya, T. Sasaki, and K. Hane, J. Vac. Sci. Technol. **33**, 031207 (2015).
[17] O. Westreich, G. Atar, Y. Paltiel, and N. Sicron, Phys. Status Solidi A **215**, 1700551 (2018).
[18] Q. Wang, R. Hui, R. Dahal, J. Y. Lin, and H. X. Jiang, Appl. Phys. Lett. **97**, 241105 (2010).
[19] Q. Wang, R. Dahal, I. W. Feng, J. Y. Lin, H. X. Jiang, and R. Hui, Appl. Phys. Lett. **99**, 121106 (2011).

[20]R. Hui, R. Xie, I. W. Feng, Z. Y. Sun, J. Y. Lin, and H. X. Jiang, Appl. Phys. Lett. **105**, 051106 (2014).

[21]I. W. Feng, W. P. Zhao, J. Li, J. Y. Lin, H. X. Jiang, and J. Zavada, Appl. Opt. **52**, 5426 (2013).

[22]Z. Y. Sun, Y. Q. Yan, T. B. Smith, W. P. Zhao, J. Li, J. Y. Lin, and H. X. Jiang, Appl. Phys. Lett. **114**, 222105 (2019).

[23]Y. Q. Yan, Z. Y. Sun, W. P. Zhao, J. Li, J. Y. Lin, and H. X. Jiang, Appl. Phys. Express **12**, 075505 (2019).

[24]U. J. Gibson, L. Wei, and J. Ballato, Nat. Commun. **12**, 3990 (2021).

[25]B. Liu and P. R. Ohodnicki, Adv. Mater. Technol. **6**, 2100125 (2021).

[26]X. Ji, S. Lei, S. Y. Yu, H. Y. Cheng, W. Liu, N. Poilvert, Y. Xiong, I. Dabo, S. E. Mohney, J. V. Badding, and V. Gopalan, ACS Photonics **4**, 85 (2017).